https://doi.org/10.5194/egusphere-2023-53
Preprint. Discussion started: 3 March 2023

The flexural isostatic response of climatically driven sea-level changes on continental-scale deltas

Sara Polanco[1], Mike Blum[2], Tristan. Salles[1], Bruce C. Frederick[2], Rebecca Farrington[3], Xuesong Ding[4], Ben Mather[1], Claire Mallard[1], Louis Moresi[5]

[1] EarthByte Group, School of Geosciences, University of Sydney, Camperdown, NSW, Australia.
[2] Earth, Energy & Environment Center, The University of Kansas, Lawrence, KS, USA.
[3] AuScope, School of Geography, Earth & Atmospheric Sciences, University of Melbourne, Parkville, VIC, Australia.
[4] Department of Earth, Planetary and Space Sciences, University of California, Los Angeles, CA, USA.
[5] Research School of Earth Sciences, Australian National University, Canberra, ACT Australia.

Correspondence to: Sara Polanco (sara.moronpolanco@sydney.edu.au)

Abstract. The interplay between climate-forced sea-level change, sediment erosion and deposition, and flexural adjustments in deep time on passive margin deltas remains poorly understood. We performed a series of conceptual simulations to investigate flexural isostatic responses to high-frequency fluctuations in water and sediment load associated with climatically driven sea-level changes. We model a large drainage basin that discharges to a continental margin to generate a deltaic depocenter, then prescribe synthetic and climatic-driven sea-level curves of different frequencies to assess flexural response. Results show that flexural isostatic adjustments are bidirectional over 100-1000 kyr timescales and are in sync with the magnitude, frequency, and direction of sea-level fluctuations, and that isostatic adjustments play an important role in driving along-strike and cross-shelf river-mouth migration and sediment accumulation. Our findings demonstrate that climate-forced sea-level changes produce a feedback mechanism that results in self-sustaining creation of accommodation into which sediment is deposited and plays a major role in delta morphology and stratigraphic architecture.

1 Introduction

The isostatic adjustments of shorelines around deltas are the result of a complex interaction of spatially-varying changes in crustal loading and unloading of sediment and water across timescales (10's Myr – 10's kyrs Watts et al., 2001). Flexural isostatic processes in large deltas reflect the accumulation of sediment loads on the crust over 10s of millions of years and are commonly treated as unidirectional at the first order over such timescales (Fig. 1; Driscoll and Karner et al., 1994; Reynolds et al., 1991; Watts et al., 2009). Over shorter time scales (10s of thousands of years) the bidirectional nature of flexural isostasy has been recognized from changes in shoreline elevations in response to crustal loading and unloading by ice during and after the last glacial maximum (e.g., the last ~30 kyrs Clark et al., 1978; Mitrovica and Peltier 1991; Lambeck et al., 2014; Whitehouse, 2018). Whereas glacial isostatic adjustments reveal the importance of water loads in creating vertical changes along shorelines, the interplay between climate-forced sea-level change, sediment erosion and deposition, and flexural

https://doi.org/10.5194/egusphere-2023-53
Preprint. Discussion started: 3 March 2023

adjustments in deep time remains poorly understood (Fig. 2, Blum et al., 2013). Moreover, the cumulative, deep-time vertical movements (10^7 to 10^8 yrs or more) that are driven by isostatic responses to sediment and water loads can have profound effects on deltaic shorelines but their effects over intermediate time scales (10^6 to 10^7 yrs) may have been underestimated. Here we use numerical models to explore how the interplay between climate-forced sea-level change, erosion and deposition, and flexural adjustments can impact the morphology, architecture and stratigraphic evolution of continental scale deltaic depocenters over these intermediate time scales (Fig. 3). The coupling of surface processes with flexural isostasy allows us to investigate feedbacks between sea-level change, erosion, deposition, flexural uplift and subsidence within a dynamic framework. Hence, we use an iterative approach because the flexural response can also generate changes in relative sea level, which in turn can modify the spatio-temporal characteristics of isostatic compensation. Our approach therefore offers a more comprehensive method than previous studies, which investigated the role of high-frequency isostatic adjustments in a static manner (Blum et al., 2008; Jouet et al., 2008).

A large body of data demonstrates close coupling over multiple time scales between climate and the globally coherent component of sea-level change that reflects global changes in ice volumes (Fig. 3; Miller et al., 2020 and references therein). Interglacial periods are characterized by lower ice volumes, higher sea level, and more landward shoreline positions, and generally result in sediment accumulation in more proximal parts of the shelf. By contrast, glacial periods are characterized by higher ice volumes, lower sea-level positions, and a corresponding basinward shift in shorelines, and generally result in the preferential transfer of sediment to the shelf margin and deep-water parts of sedimentary basins (Johannessen and Steel, 2005; Carvajal et al., 2009; Blum et al., 2008; Somme et al., 2009; Sweet and Blum, 2016; Mason et al., 2019). Bidirectional high-frequency glacio- and hydro-isostatic flexural adjustments have been extensively studied and are known to significantly impact relative sea-level histories (e.g. Clark et al., 1978; Nakada and Lambeck, 1989; Lambeck, 1995; Mitrovica and Milne, 2003; Peltier, 2004; Lambeck et al., 2014; Whitehouse, 2018). Moreover, a few studies have begun to elucidate the presence and significance of high-frequency, cyclical sediment- and hydro-isostatic adjustments associated with the response of sediment dispersal systems to climate and sea-level change. Such studies have focused on the continental scale Mississippi River delta (e.g. Ivins et al., 2007; Blum et al., 2008; Wolstencroft et al., 2014; Kuchar et al., 2018), the Rhone delta in southern France (e.g. Jouet et al., 2008) and conceptual modeling (e.g. Blum et al., 2013).

In this paper, we explore the flexural responses to sediment and water redistribution caused by climate-forced sea-level change over intermediate time scales of 10^6 to 10^7 yrs using the basin and landscape dynamics model BADLANDS (Salles and Hardiman, 2016; Salles et al., 2018). We first develop a continental-scale fluvial-deltaic to deep-water sediment-dispersal system, then perform a series of tests where we impose synthetic and climate-driven sea-level curves of different frequencies to explore the relationships between patterns of sediment accumulation, flexural subsidence, and load partitioning. Our experiments show the cumulative effect of high frequency, bidirectional flexural adjustments caused by climate-forced sea-level changes can significantly impact the morphology, architecture and stratigraphic evolution of large delta systems.

https://doi.org/10.5194/egusphere-2023-53
Preprint. Discussion started: 3 March 2023

2 Components of Vertical Motion in Passive Margin Deltaic Depocenters

To put the role of flexural isostasy in context, we first outline the nature and contribution of different processes to vertical motions over different spatio-temporal scales (Fig. 1). Accommodation from subsidence in large passive margin deltaic depocenters is generated by several processes that operate over different time scales, at different depths, and at different rates. At the largest spatial and temporal scales, vertical movements are initiated during the initial rifting phase by stretching and thinning of the lithosphere (e.g., Mackenzie, 1978; Galloway, 1989). Thermal cooling and contraction of upwelled asthenosphere then causes the margin to subside during the post-rift phase. In thermally mature passive margins with thick deltaic depocenters the amount of post-rift subsidence may exceed the possible thermal contribution, such that dynamic topography has been proposed to be a significant component (e.g., Wang et al., 2017; Wang et al., 2020).

Vertical movements during the lifespan of mature passive margin deltaic depocenters are also known to result from flexural isostatic compensation to sediment loading, which produces bending of the lithosphere (Watts et al., 2008). Published examples include the Amazon (Driscoll and Karner, 1994; Watts et al., 2008), Niger (Doust and Omatbola 1990) and Mississippi (Feng et al., 1994; Frederick et al., 2019) systems. Moreover, Driscoll and Karner (1974) initially showed that flexural subsidence from long-term depocenter sediment loading can drive the development of low-amplitude peripheral bulges 100s of km alongshore from the depocenter. We also note that hydro-isostatic adjustments result from sea-level fall and unloading of the shelf, and the inverse, sea-level rise and loading of the shelf. Blum et al. (2013) suggest that hydro-isostatic changes in response to a single cycle of sea-level fall and rise can result in changes in river gradients, as well as depth of incision and filling of coastal plain to cross-shelf valley systems.

Growth faults (e.g., Armstrong et al., 2014; Shen et al., 2016), salt tectonics (Morley et al 2011; King et al., 2012; Jackson and Hudec, 2017) and long-term compaction (Athy, 1930; Meckel et al., 2007) also contribute to long-term subsidence in deltaic depocenters: although their occurrence and activity can be related to rheological changes, subsidence patterns associated with these drivers create mechanisms that affect coastal and fluvial depositional processes on more local scales (100s to 1000s of km^2). Last, over timescales of 10^4 yrs or less, land-surface subsidence in modern large deltaic depocenters can be dominated by dewatering and consolidation of Holocene deltaic sediments within the uppermost 10s of m of strata (Tornqvist et al., 2008; Jankowski et al., 2017).

Subsidence processes on deltaic depocenters operate at different rates, and there is generally an inverse relationship between rates and the time interval over which rates are integrated (e.g. Sadler 1981, 1999). Subsidence rates associated with consolidation and dewatering of Holocene deltaic sediments are, for example, measured over annual to millennial time scales, and can be more than an order of magnitude higher than time-averaged rates associated with deep-seated subsidence mechanisms (e.g., thermal and/or dynamic subsidence, long-term loading and lithospheric flexure, and deep-seated long-term

https://doi.org/10.5194/egusphere-2023-53
Preprint. Discussion started: 3 March 2023

compaction) (see Tornqvist et al., 2008; Frederick et al., 2019). Motion on growth faults is inherently episodic, with high rates of vertical motion over short periods of time when faults are actively moving, but lower rates when integrated over longer periods of time. For the well-studied Mississippi deltaic depocenter, deep-seated components are generally <1-2 mm/yr (e.g., Frederick et al., 2019), whereas consolidation of shallow Holocene sediments can occur at rates up to an order of magnitude higher (e.g., Tornqvist et al., 2008).

3 Methods

We use BADLANDS (Salles and Hardiman, 2016; Salles et al., 2018) to explore how the interplay between climate-forced sea-level change, erosion/deposition and flexural adjustments in deep time can impact the morphology, architecture and stratigraphic evolution of continental scale deltaic depocenters. BADLANDS links landscape and basin dynamics through simulation of erosion, landscape evolution, and sedimentation. The flexural isostatic response of changes in water and sediment load is calculated using a two-way coupling between BADLANDS and *gFlex* (Wickert, 2016), which computes the flexural deflection of the Earth's surface by using an elastic plate flexure solution.

Our experimental design consists of a series of simulations where sediment is transported by hillslope and channel processes from the continental interior to the continental margin, and where river channels, deltas, shallow-marine shelves and shelf margins are self-generated. Landscape dynamics are controlled by local gradient, water discharge, sediment flux and flexural adjustments. Our simulations produce catchment areas, river lengths, and volumes of deposited sediment that are consistent with the ranges observed in continental-scale source-to-sink systems such as the Mississippi and Amazon rivers (Fig.4). We do not aim to reproduce the geological history of a particular continental-scale source-to-sink system, our goal is to better understand first-order relationships between sea-level changes, flexural isostasy, and erosion and deposition.

The initial configuration of the modeling domain resembles the topography of a natural source-to-sink system with 3400 m elevation in the headwaters, a length of 4500 km, a downstream-decreasing fluvial channel slope, and successive inflections in gradient associated with the coastal-plain to continental shelf and shelf to slope transitions (Fig. 4a, S1). To ensure that our simulated drainage basin produces a point-source for sediment input to the marine domain we imposed a longitudinal topographic low in the middle of the model. The resultant drainage basin and associated deltaic depocenter are then self-formed (Fig. 4a) as the result of the imposed uniform precipitation, continental and marine surface processes forcings. The similarity between simulated river length and catchment area and large-scale natural source-to-sink systems (Fig. 4b) supports the choices made for our initial settings and allows us to draw relationships between simulated results and natural systems. The three-dimensional spatial mesh size and temporal resolution were chosen to adequately reproduce the first-order geomorphological and architectural evolution of deltaic systems (Fig. 4c) and to ensure that the frequency of sea-level fluctuations is adequately

https://doi.org/10.5194/egusphere-2023-53
Preprint. Discussion started: 3 March 2023

captured. Details about boundary conditions and input parameters used in modeling simulations can be found in Table 1 and the data repository.

We perform a series of simulations where we first hold sea level constant, then impose synthetic and climate-forced sea-level curves. Synthetic curves were constructed to reflect frequencies of 500 kyr and 5 Myr, whereas climate-forced sea-level curves were selected from intervals in geologic time with contrasting climatic regimes and therefore contrasting sea-level amplitudes and directions: we extracted data from Miller et al. (2020) that correspond to the generally ice-free Paleocene-Eocene, ca. 66-56 Ma (hereafter greenhouse) and the ice-dominated Oligocene ca. 33.9-23.9 Ma (icehouse) periods (Fig. 3 b, c). These simulations are then compared to a suite of non-flexurally-compensated models. The sea-level curves we use are resampled to time steps of 50 kyr with outputs generated every 100 kyrs. We let each simulation initialize and run for 2 Myr without any sea-level fluctuations so that the delta can reach dynamic equilibrium without any disturbances in base level, then impose both the synthetic and climate-forced sea-level changes.

For flexurally-compensated models, we use an effective elastic thickness (Te) of 50 km.
This value is within the range observed in passive margins (Tesauro et al., 2012) and similar values have been used in previous flexural studies of continental-scale deltaic depocenters (e.g. Driscoll and Karner 1994; Watts et al., 2009). We test the sensitivity to Te by running a series of simulations where Te varies from 10 to 100 km. Results from the sensitivity analysis show a similar pattern in the flexural response when using Te values lower than 60 km, whereas larger values result in a lower flexural amplitude and larger flexural wavelength (Fig. S2), which is in accordance with observations made for rigid lithosphere found in cratonic regions (Tesauro et al., 2012). We chose a spatially uniform value of Te in all simulations and therefore do not account for possible spatial variations in lithospheric rigidity that could generate small differences in flexural deflections. However, we consider such differences to be negligible compared to the flexural adjustments caused by the large sediment loads typical of passive margins. To ensure the computed flexural response is in-phase with our imposed sea-level cycles, we use a temporal resolution of 100 kyr to compute isostatic flexure. We have conducted sensitivity tests with higher temporal resolution for both sea level and flexural response (up to 10 kyr) as well, and similar behaviors to those presented here emerged.

Our simulations hold precipitation constant over time, and do not include tectonic or dynamic uplift in upstream regions, or lithological changes in subsurface sedimentary layers. Such parameters clearly play a role in the sediment volumes and rates delivered to the marine environment, and therefore the accumulated sediment load, but are not considered here to avoid complicating the analysis of the effect of high-frequency, high-resolution isostatic adjustments to changes in crustal loading due to both the sediment and water load, the primary effect that we aim to unravel in this paper. Our simulations also do not account for sediment compaction or sediments of different grain sizes.

https://doi.org/10.5194/egusphere-2023-53
Preprint. Discussion started: 3 March 2023

4 Results and discussion

Our results focus on how the interplay between flexural adjustments erosion/deposition and climate-forced sea-level change in deep time can significantly impact the morphology, architecture and stratigraphic evolution of continental scale deltaic depocenters. Below, we highlight three distinct results: (a) flexural effects on the morphology and stratigraphy of large deltas, (b) the relationships between flexural adjustments and sea-level change, and how they impact delta morphology, and (c) the hydro-isostatic effects on delta morphology and stratigraphy.

4.1 Flexural isostatic effects on delta morphology and stratigraphic evolution

Our simulations show that cyclical flexural isostatic adjustments in response to sea-level change impact generation of the stratigraphic record through changes in river-mouth cross-shelf transit distances, river mouth lateral migration, and patterns of accommodation. In all simulations, mean river-mouth transit distances and lateral river-mouth migration distances are significantly greater in non-flexurally-compensated simulations when compared to their flexurally-compensated counterparts (Table 2; Figs. 5, 7). We attribute these patterns to reduced accommodation when flexural compensation is absent, which, in turn, limits sediment accumulation close to the river mouth, forces the delta to prograde farther into the coastal ocean, and forces the river channel to migrate laterally away from older deposits (Fig. 5 m-o). Conversely, in simulations with flexural compensation, accommodation increases near the delta front as the load accumulates, which reduces cross-shelf transit distances and lateral migration of the river channel (Fig. 5 j-l). Mean maximum rates of sediment accumulation at the river mouth, an indicator of accommodation that has been generated, are significantly smaller in non-flexurally compensated simulations when compared to their flexurally compensated counterparts (see Table 2). Furthermore, our simulations show a correspondence between river-mouth cross-shelf transit distances and the sea-level position (Fig. 6), confirming the role that sea level plays as the main driver on the sediment dispersal of passive margins (e.g. Carvajal et al., 2009; Sømme et al., 2009).

4.2 Interplay between flexural adjustments and sea-level change in delta morphology

We find that simulations where we impose synthetic sea-level changes show that flexural adjustments are not unidirectional and instead can be bidirectional at a rate of change and direction that amplifies the sea-level fluctuations themselves. These results demonstrate that significant bidirectional flexural compensation can take place at high frequencies, in this case with sea-level cycles of 500 kyr and 5 Myr (Fig. 5 e-f). In each case there is a background monotonic increase in the accumulated flexural subsidence as the sediment load increases through time, but flexure is uniformly unidirectional if and only if sea level is held constant (Fig. 5d). The synchronicity between sea-level change and flexural response is confirmed by spectral analyses that show peaks at frequencies that are similar to the imposed synthetic sea-level fluctuations and flexural response at the river mouth (Fig. 5). Simulations that use climate-driven empirical sea-level curves also show that flexural response is both cyclical and in-phase with the frequencies and amplitudes of sea-level fluctuations (Fig. 7), and thus reflects climate-driven changes in sediment loading and thickness of the water column.

https://doi.org/10.5194/egusphere-2023-53
Preprint. Discussion started: 3 March 2023

The synthetic stratigraphy produced by our simulations records the coupled forcing of climate-driven sea-level change, flexural compensation, and generation of accommodation, which in turn drives river mouth lateral migration and cross-shelf transit distances (Fig. 5 j-i, m-o; Fig. 7 g-j). Simulations without flexural compensation show a larger proportion of hiatuses in the stratigraphic record when compared to flexurally-compensated simulations (Figs. 5, 7, 8). Flexurally-compensated simulations with no sea-level change record a simple normal regression (Fig. 5j), whereas simulations with imposed synthetic and empirical sea-level curves display significant hiatuses during sea-level fall and forced regression of the river mouth (sensu Posamentier & Allen, 1999), but fewer hiatuses during sea-level rise when the river mouth and shoreline migrate landwards. In a natural system, such changes would be analogous to the net valley incision and cross-shelf extension of river systems that accompanies sea-level fall or, conversely, the valley aggradation and filling that accompanies shortening of the river system as the shoreline steps landward during sea-level rise (Fig. 5 k-i, ho; Fig. 7 g-j, Fig. 8, 9). Simulations with higher amplitude icehouse sea-level curves show a higher number of erosional hiatuses when compared to simulations with lower amplitude greenhouse sea-level curves. We attribute this observation to reflect more frequent subaerial exposure of the shelf during icehouse climates, and less frequent exposure in the greenhouse case (Fig. 7, 8).

4.3 Hydro-isostatic effects on delta morphology and stratigraphic evolution

Isostatic compensation to changes in water load also plays a role in the spatio-temporal evolution of large deltas. We computed the change in the water column in the marine part of the modeling domain for each time step and then calculated hydro-isostatic responses in gFlex (Wickert 2016). We chose this approach because BADLANDS and gFlex are fully coupled to calculate the flexural isostatic compensation of both the sediment and water load, so we extracted the water load component in the post-processing stage. As expected, our results show that spatial variation in hydro-isostatic adjustments is a function of the magnitude and frequency of sea-level change, and related to the progradation of deltaic sediment wedges (Fig. 10-13). For instance, it is well known from the Quaternary that shelf-margin width and depth changes in response to climate-driven sea-level change (e.g., Blum and Womack, 2009; Blum et al., 2013): when sea level is low, the deltaic shoreline is located proximal to the shelf margin in shallow water depths, and the shelf is generally narrow, whereas when sea level is high, the shelf may be 100s of km wide and offshore, in water depths of 100 m or more. Our results are consistent with earlier 1-D modeling results in Blum et al. (2013), which show that hydro-isostatic uplift in response to sea-level fall will impact river long profiles, and will enhance the depth of incision in a wide shelf setting, whereas hydro-isostatic subsidence in response to sea-level rise will enhance accommodation and result in increased aggradation.

By incorporating the effects of erosion and deposition in a dynamic manner, our simulations allow to investigate the cumulative effects of the feedbacks between hydro-isostasy and erosion/deposition. In the ice-house scenario, with high amplitude sea-level changes, the shelf slope is steeper as a result of (i) the back-and-forth cross-shelf transit of river mouths and (ii) the amplification of valley incision by hydro-isostatic uplift. In the greenhouse scenario, with low amplitude sea-level changes,

https://doi.org/10.5194/egusphere-2023-53
Preprint. Discussion started: 3 March 2023

the shelf is inherently narrow, and the shoreline remains proximal to the shelf margin: the slope of the shelf is shallower than in the ice-house case because of relatively continuous and widespread delta topset aggradation. Our modelled scenario with no sea-level changes exhibits the greatest degree of progradation of the river mouth, shelf margin, and slope: without flexural compensation, the final elevation of the coastal plain is therefore a result of the initial topography, erosion, and base-level changes (Fig. 14, 15).

Our simulations demonstrate the potential role of high-frequency climate-forced sea-level changes in generating high-frequency flexural responses, because they drive changes in the location and volume of fluvial-deltaic sediment accumulation. Our results also show that accommodation is not first created and then filled later, but instead coevolves in-sync with responses of fluvio-deltaic systems to climate-driven sea-level change. Indeed, the short time scales over which significant flexural response can take place makes it likely that sediment- and hydroisostasic flexural adjustments represent dynamic controls that affect the behavior of fluvial and deltaic systems in real time. Flexural uplift from sediment- and hydro-isostatic unloading of the shelf during climate-driven sea-level fall likely promotes enhanced incision and drives the formation of hiatuses as the river mouth transits across the subaerially-exposed shelf. On the other hand, sediment- and hydro-isostatic loading of the shelf during climate-driven sea-level rise results in increased accommodation and sediment accumulation. In this way, climate-forced sea-level changes set up a feedback mechanism that results in self-sustaining destruction of accommodation and generation of hiatuses during sea-level fall, and self-sustaining creation of accommodation and sediment accumulation during sea-level rise.

Last, we note that our work focuses on passive margins, but the dynamic relationship between flexure, river-mouth transit distances and accommodation should occur in basin settings with high elastic thickness as well. For example, an especially rigid lithosphere would limit the deltaic accommodation generated by the vertical component of flexure, significant fluvial-deltaic stratal thicknesses will not accumulate, and river mouth transit distances in response to sea-level change will necessarily be very large.

5 Conclusions

We use conceptual simulations to unravel the interplay between climate-forced sea-level change, sediment erosion and deposition, and flexural adjustments in deep time on passive margin deltas. Our results illustrate how cumulative high-frequency, bidirectional isostatic adjustments play an important role in driving along-strike and cross-shelf river-mouth migration and sediment accumulation. Our results also add a different dimension to the widely-accepted view that accommodation is first created and then infilled, instead our experiments show that accommodation coevolves in-sync with responses of fluvio-deltaic systems and flexural isostatic adjustments to climate-driven sea-level change. In our case, we find that only simulations with no imposed sea-level change produce a true monotonic increase in flexural subsidence and

https://doi.org/10.5194/egusphere-2023-53
Preprint. Discussion started: 3 March 2023

unidirectional deltaic progradation, regardless of time scale. We therefore view cyclical and bidirectional flexural responses to be inherent in fluvio-deltaic systems because they are coupled to the increasingly well-understood nature of how surface dynamics in fluvial-deltaic systems respond to climate-forced sea-level changes to produce the stratigraphic record.

Acknowledgments

This research was supported by Australian Research Council's ITRH project IH130200012. SM acknowledges support from the University of Melbourne Early Career Researcher and mobility grants as well as a travel grant from the Australian Academy of Science to work with M. Blum and B. Frederick at the University of Kansas. The authors thank A. Wickert and an anonymous reviewer for their constructive comments on an earlier version of this manuscript.

References

Armstrong, C., Mohrig, D., Hess, T., George, T., and Straub, K. M.: Influence of growth faults on coastal fluvial systems: Examples from the late Miocene to Recent Mississippi River Delta, Sedimentary Geology, 301, 120-132, https://doi.org/10.1016/j.sedgeo.2013.06.010, 2014.

Athy, L. F.: Density, Porosity, and Compaction of Sedimentary Rocks1, AAPG Bulletin, 14, 1-24, 10.1306/3d93289e-16b1-11d7-8645000102c1865d, 1930.

Blum, M., Martin, J., Milliken, K., and Garvin, M.: Paleovalley systems: Insights from Quaternary analogs and experiments, Earth-Science Reviews, 116, 128-169, https://doi.org/10.1016/j.earscirev.2012.09.003, 2013.

Blum, M. D., Tomkin, J. H., Purcell, A., and Lancaster, R. R.: Ups and downs of the Mississippi Delta, Geology, 36, 675-678, 10.1130/g24728a.1, 2008.

Blum, M. D., Hattier-Womack, J., Kneller, B., Martinsen, O. J., and McCaffrey, B.: Climate Change, Sea-Level Change, and Fluvial Sediment Supply to Deepwater Depositional Systems, in: External Controls on Deep-Water Depositional Systems, SEPM Society for Sedimentary Geology, 0, 2009.

Carvajal, C., Steel, R., and Petter, A.: Sediment supply: The main driver of shelf-margin growth, Earth-Science Reviews, 96, 221-248, https://doi.org/10.1016/j.earscirev.2009.06.008, 2009.

Clark, J. A., Farrell, W. E., and Peltier, W. R.: Global changes in postglacial sea level: A numerical calculation, Quaternary Research, 9, 265-287, https://doi.org/10.1016/0033-5894(78)90033-9, 1978.

Doust, H., and Omatbola, E.: Niger Delta, in: Divergent/Passive Margin Basins, 2009/05/01 ed., edited by: Edwards, J. D., and Santogrossi, P. A., AAPG, 201-238, 1990.

Driscoll, N. W., and Karner, G. D.: Flexural deformation due to Amazon Fan loading: A feedback mechanism affecting sediment delivery to margins, Geology, 22, 1015-1018, 10.1130/0091-7613(1994)022<1015:Fddtaf>2.3.Co;2, 1994.

Feng, J., Buffler, R. T., and Kominz, M. A.: Laramide orogenic influence on late Mesozoic-Cenozoic subsidence history, western deep Gulf of Mexico basin, Geology, 22, 359-362, 10.1130/0091-7613(1994)022<0359:Loiolm>2.3.Co;2, 1994.

Frederick, B. C., Blum, M., Fillon, R., and Roberts, H.: Resolving the contributing factors to Mississippi Delta subsidence: Past and Present, Basin Research, 31, 171-190, https://doi.org/10.1111/bre.12314, 2019.

Galloway, W. E.: Genetic Stratigraphic Sequences in Basin Analysis II: Application to Northwest Gulf of Mexico Cenozoic Basin1, AAPG Bulletin, 73, 143-154, 10.1306/703c9afa-1707-11d7-8645000102c1865d, 1989.

Ivins, E. R., Dokka, R. K., and Blom, R. G.: Post-glacial sediment load and subsidence in coastal Louisiana, Geophysical Research Letters, 34, https://doi.org/10.1029/2007GL030003, 2007.

Jackson, M. P. A., and Hudec, M. R.: Salt Tectonics: Principles and Practice, Cambridge University Press, Cambridge, 2017.

Jankowski, K. L., Törnqvist, T. E., and Fernandes, A. M.: Vulnerability of Louisiana's coastal wetlands to present-day rates of relative sea-level rise, Nature Communications, 8, 14792, 10.1038/ncomms14792, 2017.

https://doi.org/10.5194/egusphere-2023-53
Preprint. Discussion started: 3 March 2023

Johannessen, E. P., and Steel, R. J.: Shelf-margin clinoforms and prediction of deepwater sands, Basin Research, 17, 521-550, https://doi.org/10.1111/j.1365-2117.2005.00278.x, 2005.

Jouet, G., Hutton, E. W. H., Syvitski, J. P. M., and Berné, S.: Response of the Rhône deltaic margin to loading and subsidence during the last climatic cycle, Computers & Geosciences, 34, 1338-1357, https://doi.org/10.1016/j.cageo.2008.02.003, 2008.

King, R., Backé, G., Tingay, M., Hillis, R., and Mildren, S.: Stress deflections around salt diapirs in the Gulf of Mexico, Geological Society, London, Special Publications, 367, 141-153, 10.1144/SP367.10, 2012.

Kuchar, J., Milne, G., Wolstencroft, M., Love, R., Tarasov, L., and Hijma, M.: The Influence of Sediment Isostatic Adjustment on Sea Level Change and Land Motion Along the U.S. Gulf Coast, Journal of Geophysical Research: Solid Earth, 123, 780-796, https://doi.org/10.1002/2017JB014695, 2018.

Lambeck, K.: Glacial isostasy and water depths in the Late Devensian and Holocene on the Scottish Shelf west of the Outer Hebrides, Journal of Quaternary Science, 10, 83-86, https://doi.org/10.1002/jqs.3390100109, 1995.

Lambeck, K., Rouby, H., Purcell, A., Sun, Y., and Sambridge, M.: Sea level and global ice volumes from the Last Glacial Maximum to the Holocene, Proceedings of the National Academy of Sciences, 111, 15296-15303, doi:10.1073/pnas.1411762111, 2014.

Mason, C. C., Romans, B. W., Stockli, D. F., Mapes, R. W., and Fildani, A.: Detrital zircons reveal sea-level and hydroclimate controls on Amazon River to deep-sea fan sediment transfer, Geology, 47, 563-567, 10.1130/g45852.1, 2019.

McKenzie, D.: Some remarks on the development of sedimentary basins, Earth and Planetary Science Letters, 40, 25-32, https://doi.org/10.1016/0012-821X(78)90071-7, 1978.

Meckel, T. A., Ten Brink, U. S., and Williams, S. J.: Sediment compaction rates and subsidence in deltaic plains: numerical constraints and stratigraphic influences, Basin Research, 19, 19-31, https://doi.org/10.1111/j.1365-2117.2006.00310.x, 2007.

Miller, K. G., Browning, J. V., Schmelz, W. J., Kopp, R. E., Mountain, G. S., and Wright, J. D.: Cenozoic sea-level and cryospheric evolution from deep-sea geochemical and continental margin records, Science Advances, 6, eaaz1346, doi:10.1126/sciadv.aaz1346, 2020.

Mitrovica, J. X., and Peltier, W. R.: On postglacial geoid subsidence over the equatorial oceans, Journal of Geophysical Research: Solid Earth, 96, 20053-20071, https://doi.org/10.1029/91JB01284, 1991.

Mitrovica, J. X., and Milne, G. A.: On post-glacial sea level: I. General theory, Geophysical Journal International, 154, 253-267, https://doi.org/10.1046/j.1365-246X.2003.01942.x, 2003.

Morley, C. K., King, R., Hillis, R., Tingay, M., and Backe, G.: Deepwater fold and thrust belt classification, tectonics, structure and hydrocarbon prospectivity: A review, Earth-Science Reviews, 104, 41-91, https://doi.org/10.1016/j.earscirev.2010.09.010, 2011.

Nakada, M., and Lambeck, K.: Late Pleistocene and Holocene sea-level change in the Australian region and mantle rheology, Geophysical Journal International, 96, 497-517, 10.1111/j.1365-246X.1989.tb06010.x, 1989.

Peltier, W. R.: GLOBAL GLACIAL ISOSTASY AND THE SURFACE OF THE ICE-AGE EARTH: The ICE-5G (VM2) Model and GRACE, Annual Review of Earth and Planetary Sciences, 32, 111-149, 10.1146/annurev.earth.32.082503.144359, 2004.

Posarnentier, H. W., and Allen, G. P.: Siliciclastic Sequence Stratigraphy—Concepts and Applications, SEPM Society for Sedimentary Geology, 1999.

Reynolds, D. J., Steckler, M. S., and Coakley, B. J.: The role of the sediment load in sequence stratigraphy: The influence of flexural isostasy and compaction, Journal of Geophysical Research: Solid Earth, 96, 6931-6949, https://doi.org/10.1029/90JB01914, 1991.

Sadler, P.: The influence of hiatuses on sediment accumulation rates, GeoResearch Forum, 1999, 15-40,

Sadler, P. M.: Sediment Accumulation Rates and the Completeness of Stratigraphic Sections, The Journal of Geology, 89, 569-584, 1981.

Salles, T., and Hardiman, L.: Badlands: An open-source, flexible and parallel framework to study landscape dynamics, Computers & Geosciences, 91, 77-89, https://doi.org/10.1016/j.cageo.2016.03.011, 2016.

Salles, T., Ding, X., and Brocard, G.: pyBadlands: A framework to simulate sediment transport, landscape dynamics and basin stratigraphic evolution through space and time, PLOS ONE, 13, e0195557, 10.1371/journal.pone.0195557, 2018.

https://doi.org/10.5194/egusphere-2023-53
Preprint. Discussion started: 3 March 2023

Shen, Z., Dawers, N. H., Törnqvist, T. E., Gasparini, N. M., Hijma, M. P., and Mauz, B.: Mechanisms of late Quaternary fault throw-rate variability along the north central Gulf of Mexico coast: implications for coastal subsidence, Basin Research, 29, 557-570, https://doi.org/10.1111/bre.12184, 2017.

Sømme, T. O., Helland-Hansen, W., Martinsen, O. J., and Thurmond, J. B.: Relationships between morphological and sedimentological parameters in source-to-sink systems: a basis for predicting semi-quantitative characteristics in subsurface systems, Basin Research, 21, 361-387, https://doi.org/10.1111/j.1365-2117.2009.00397.x, 2009.

Sweet, M. L., and Blum, M. D.: Connections Between Fluvial To Shallow Marine Environments and Submarine Canyons: Implications For Sediment Transfer To Deep Water, Journal of Sedimentary Research, 86, 1147-1162, 10.2110/jsr.2016.64, 2016.

Tesauro, M., Kaban, M. K., and Cloetingh, S. A. P. L.: Global strength and elastic thickness of the lithosphere, Global and Planetary Change, 90-91, 51-57, https://doi.org/10.1016/j.gloplacha.2011.12.003, 2012.

Törnqvist, T. E., Wallace, D. J., Storms, J. E. A., Wallinga, J., van Dam, R. L., Blaauw, M., Derksen, M. S., Klerks, C. J. W., Meijneken, C., and Snijders, E. M. A.: Mississippi Delta subsidence primarily caused by compaction of Holocene strata, Nature Geoscience, 1, 173-176, 10.1038/ngeo129, 2008.

Wang, H., Gurnis, M., and Skogseid, J.: Rapid Cenozoic Subsidence in the Gulf of Mexico Resulting From Hess Rise Conjugate Subduction, Geophysical Research Letters, 44, 10,930-910,938, https://doi.org/10.1002/2017GL074959, 2017.

Wang, H., Gurnis, M., and Skogseid, J.: Continent-wide drainage reorganization in North America driven by mantle flow, Earth and Planetary Science Letters, 530, 115910, https://doi.org/10.1016/j.epsl.2019.115910, 2020.

Watts, A. B.: Isostasy and Flexure of the Lithosphere, New York, 2001.

Watts, A. B., Rodger, M., Peirce, C., Greenroyd, C. J., and Hobbs, R. W.: Seismic structure, gravity anomalies, and flexure of the Amazon continental margin, NE Brazil, Journal of Geophysical Research: Solid Earth, 114, https://doi.org/10.1029/2008JB006259, 2009.

Whitehouse, P. L.: Glacial isostatic adjustment modelling: historical perspectives, recent advances, and future directions, Earth Surf. Dynam., 6, 401-429, 10.5194/esurf-6-401-2018, 2018.

Wickert, A. D.: Open-source modular solutions for flexural isostasy: gFlex v1.0, Geosci. Model Dev., 9, 997-1017, 10.5194/gmd-9-997-2016, 2016.

Wolstencroft, M., Shen, Z., Törnqvist, T. E., Milne, G. A., and Kulp, M.: Understanding subsidence in the Mississippi Delta region due to sediment, ice, and ocean loading: Insights from geophysical modeling, Journal of Geophysical Research: Solid Earth, 119, 3838-3856, https://doi.org/10.1002/2013JB010928, 2014.

https://doi.org/10.5194/egusphere-2023-53
Preprint. Discussion started: 3 March 2023

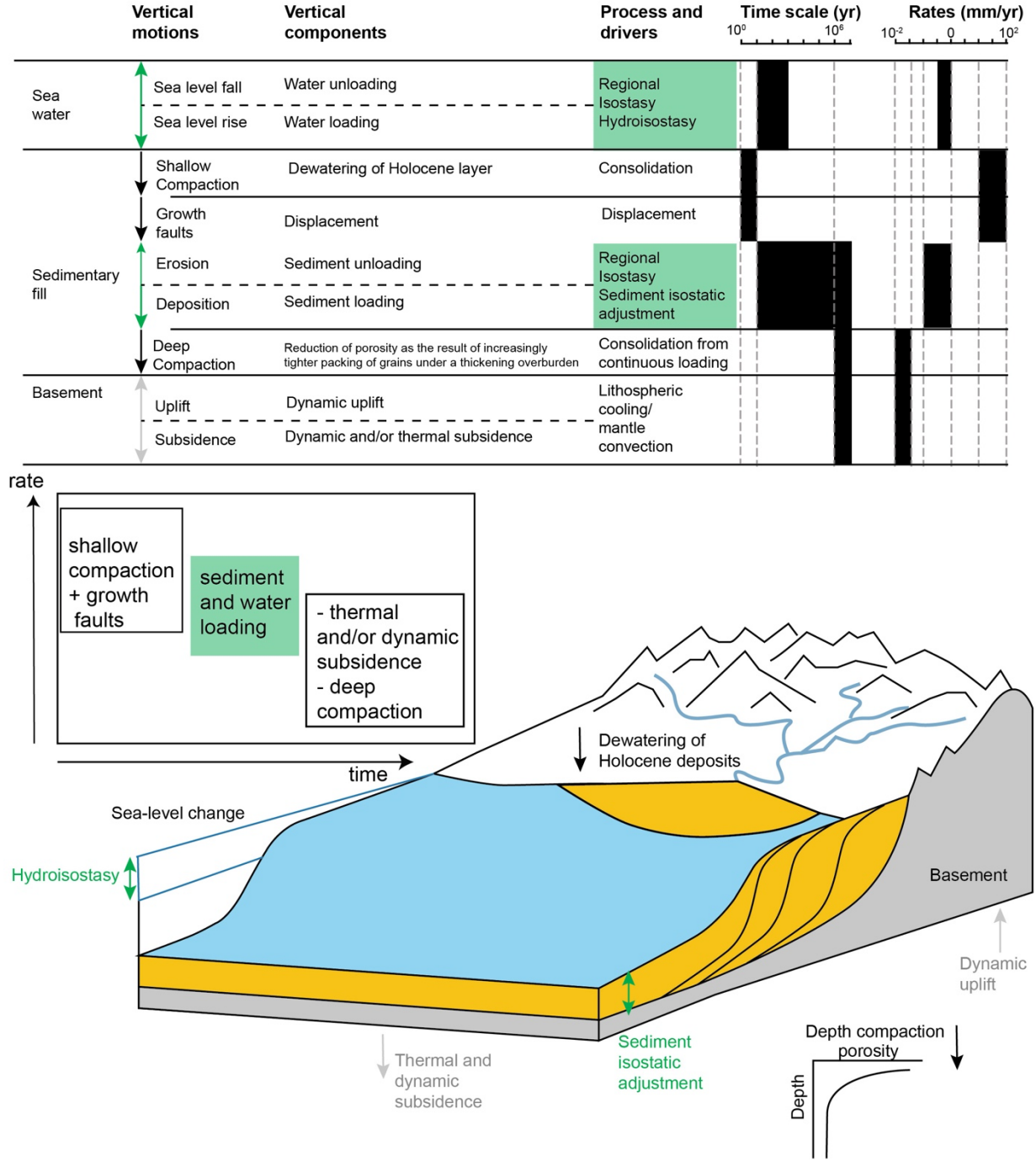

380

Figure 1. Figure showing the components of vertical motions in passive margins with deltaic depocenters at different spatio-temporal scales. Rates of vertical motions are from Allen and Allen (2005); Jouet et al., (2008) and Frederick et al., (2019). Note that tectonic uplift and subsidence are not included because our study focuses on passive margins.

https://doi.org/10.5194/egusphere-2023-53
Preprint. Discussion started: 3 March 2023

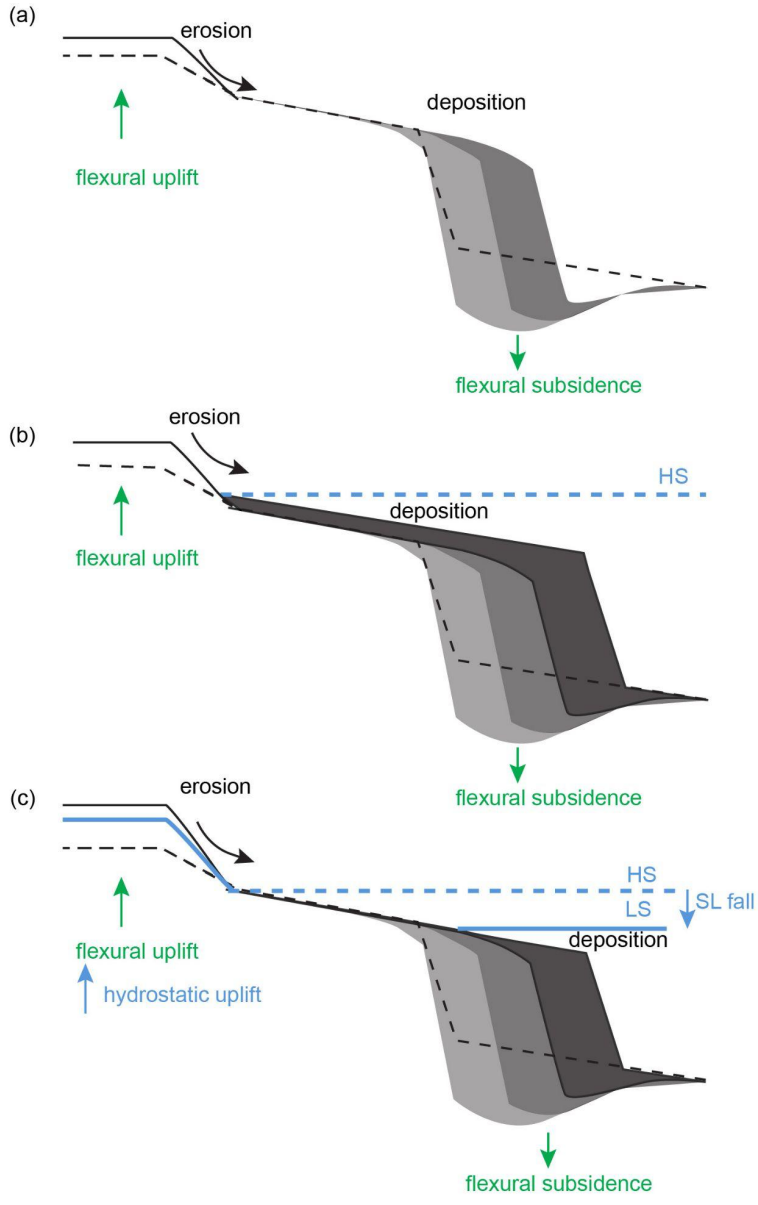

385 **Figure 2. Conceptual model for the complex interaction between surface processes (erosion and deposition), the progressive flexure of the lithosphere due to (a) prograding sediment load and (b-c) hydro-isostasy due to sea-level changes. Note how the position of the sediment load changes with the position of the sea level and how hydrostatic uplift takes place as a result of sea-level (SL) fall. HS=High stand, LS= Low stand. Modified from Watts (1989).**

390

https://doi.org/10.5194/egusphere-2023-53
Preprint. Discussion started: 3 March 2023

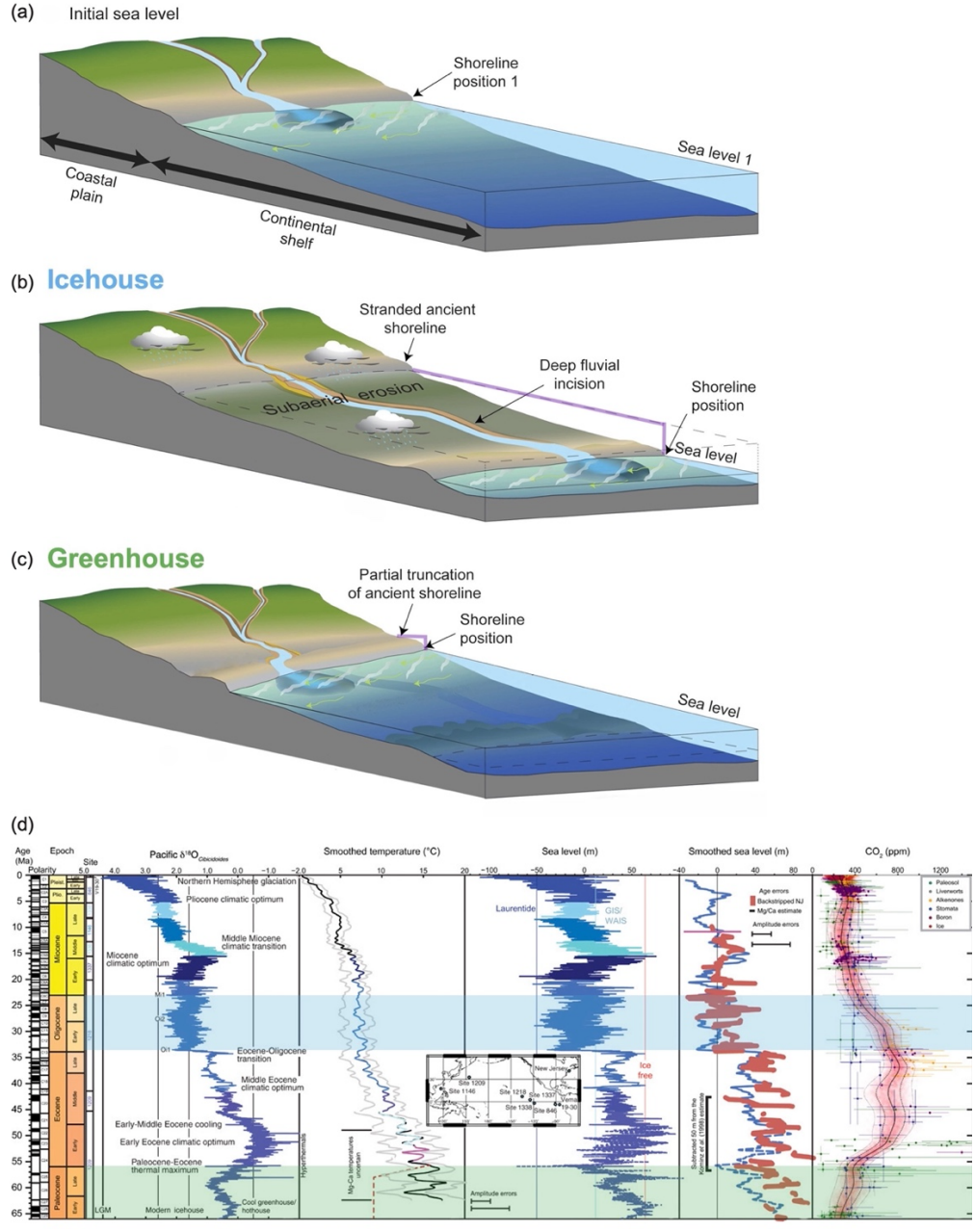

Figure 3. Conceptual model for the evolution of (a) deltaic depocenters in response to sea level changes during (b) icehouse and (c) greenhouse periods. The frequent and large amplitude variation of the sea-level (purple line) during icehouse periods results in the exposure of the continental shelf and deep fluvial incision and sediment loads being deposited deep into the basin. In contrast, during greenhouse periods the smaller amplitude of the sea-level variation (purple line) results in sediment being deposited closer to the continent. We test the isostatic response of the aforementioned water and sediment partitioning. Figure modified from https://pubs.usgs.gov. (d) Summary of Cenozoic benthic foraminiferal $\delta^{18}O$, temperature and sea level showing the selected sea-level curves from ice-free (Paleocene-Eocene, ca. 66-56 Ma) and ice-dominated (Oligocene ca. 33.9-23.9 Ma) periods, modified from Miller et al., (2020).

https://doi.org/10.5194/egusphere-2023-53
Preprint. Discussion started: 3 March 2023

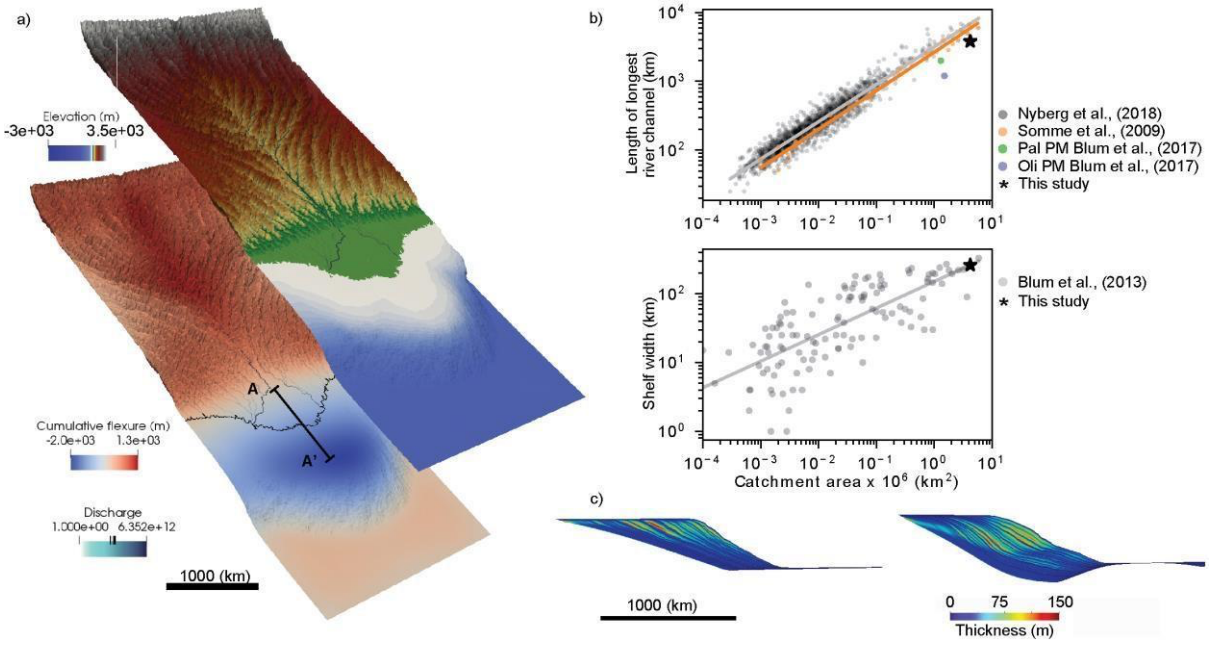

Figure 4. (a) Example outputs from numerical simulations that show elevation and bathymetry (top) and cumulative flexure (bottom). Model dimensions are 4500 km x 2000 km, with a vertical exaggeration of 100x. (b) Scatter plot of river length (top) and shelf width (bottom) versus catchment area from river systems. Data is from Somme et al. (2009), Nyberg et al. (2018), Blum et al. (2013, 2017) and simulations presented in this study. Pal= Paleocene, Oli=Oligocene, PM= Paleo-Mississippi. (c) Example of synthetic stratigraphy from a simulation without (left) and with flexural compensation (right). Vertical exaggeration is 150x. Wheeler diagrams presented in Figures 5 and 7 were constructed along cross-section A-A'.

https://doi.org/10.5194/egusphere-2023-53
Preprint. Discussion started: 3 March 2023

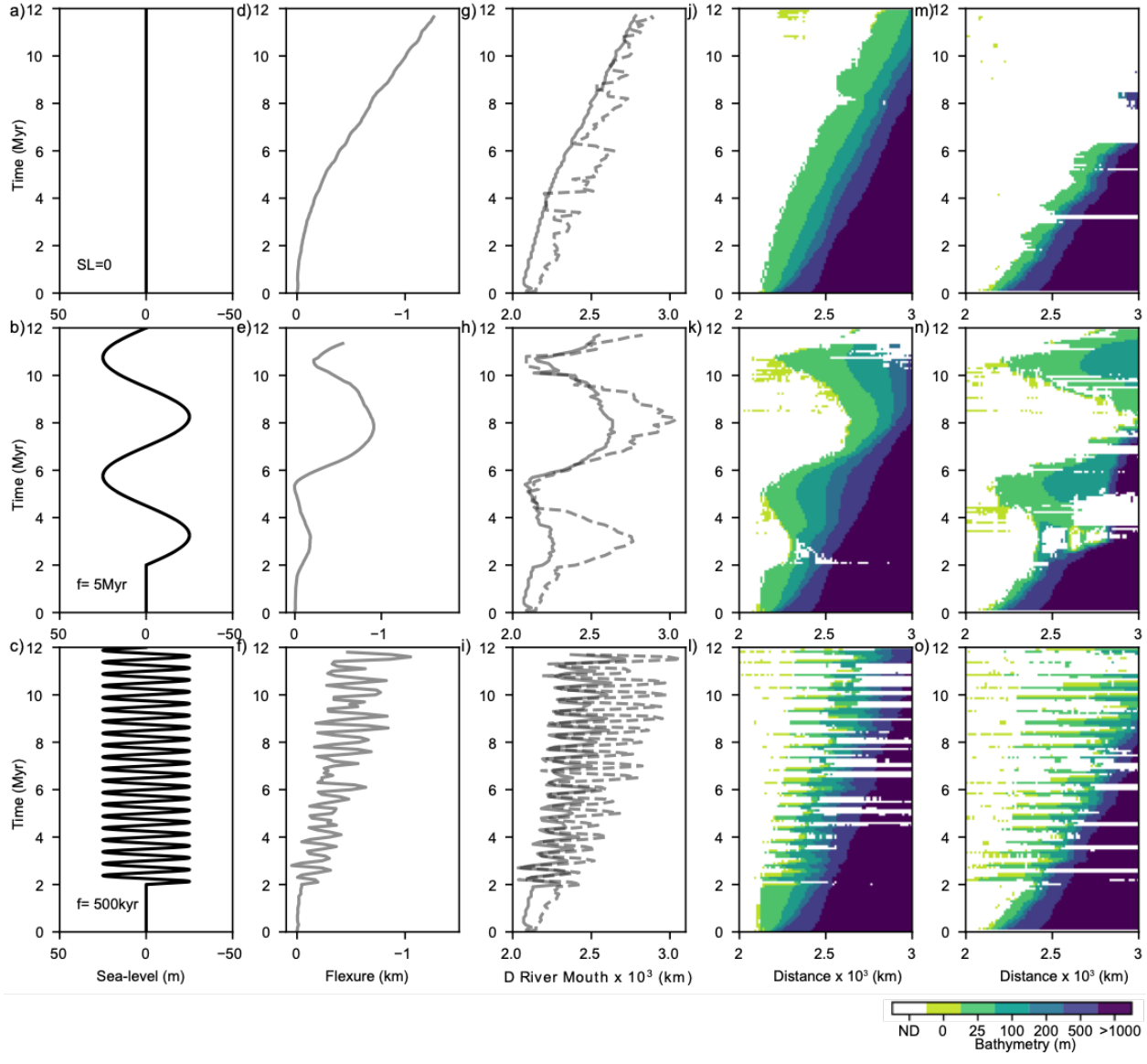

Figure 5. Synthetic sea-level curves (a-c), computed flexural deflection through time (d-f), travel distance of the river mouth (g-i) and Wheeler diagrams for the flexurally compensated (j-l) and non-flexurally compensated (m-o) simulations. The location of the cross-section used to construct the Wheeler diagram is shown in Figure 1. Wheeler diagrams are constructed using the post-processing module of BADLANDS (Salles et al., 2018). ND= No deposition.

https://doi.org/10.5194/egusphere-2023-53
Preprint. Discussion started: 3 March 2023

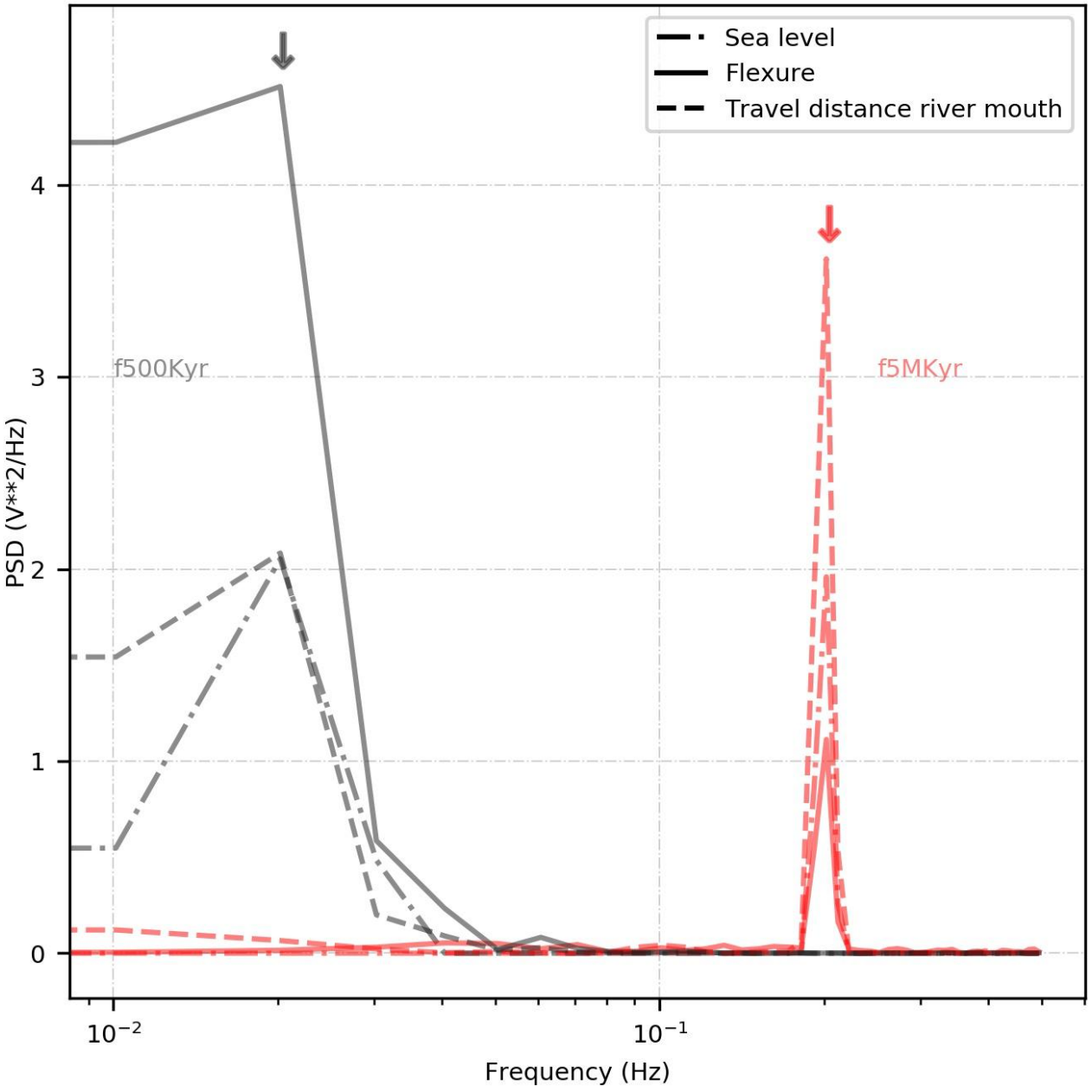

Figure 6. Power-spectral density (PSD) for simulations with a frequency of 5 Myr (grey) and 500 kyr (red). Correspondence in peak frequencies between sea level, flexural deflection and river mouth migration provides further evidence to demonstrate that flexural deflection and flexural subsidence are in-phase with sea-level changes.

https://doi.org/10.5194/egusphere-2023-53
Preprint. Discussion started: 3 March 2023

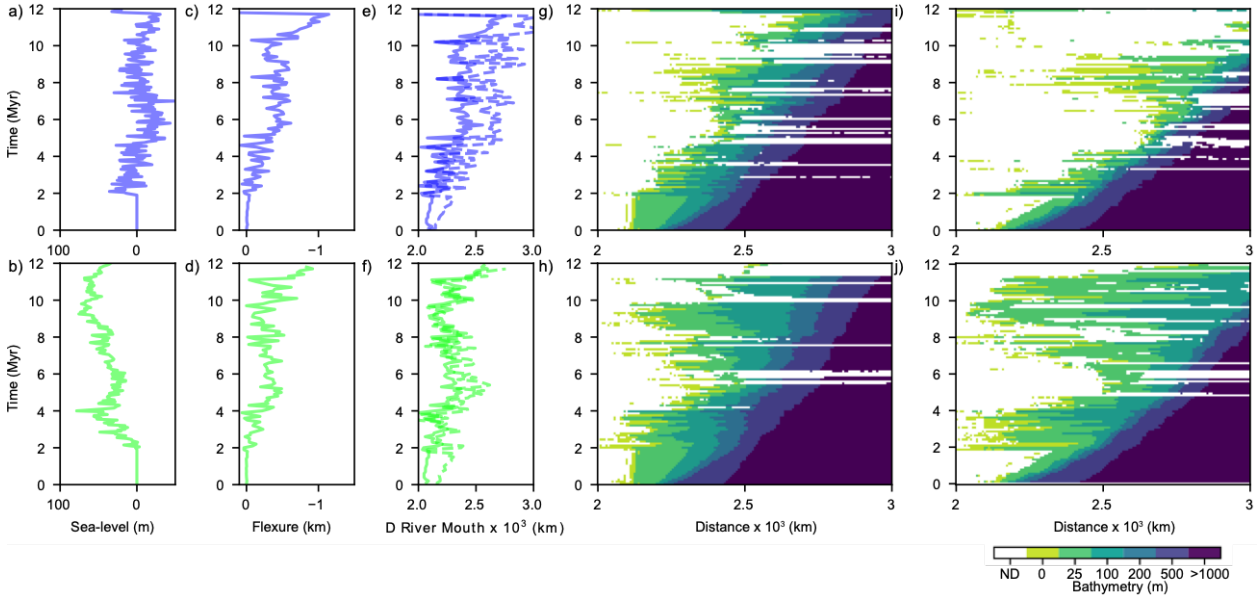

Figure 7. Outputs of numerical simulations that represent Ice-house (top) and Green-house periods (bottom). (a-b) sea-level curves, (c-d)computed flexural deflection, (e-f) travel distance of the river mouth. Wheeler diagrams for flexurally compensated models (g-h) and (i-j) non-flexural counterparts.

https://doi.org/10.5194/egusphere-2023-53
Preprint. Discussion started: 3 March 2023

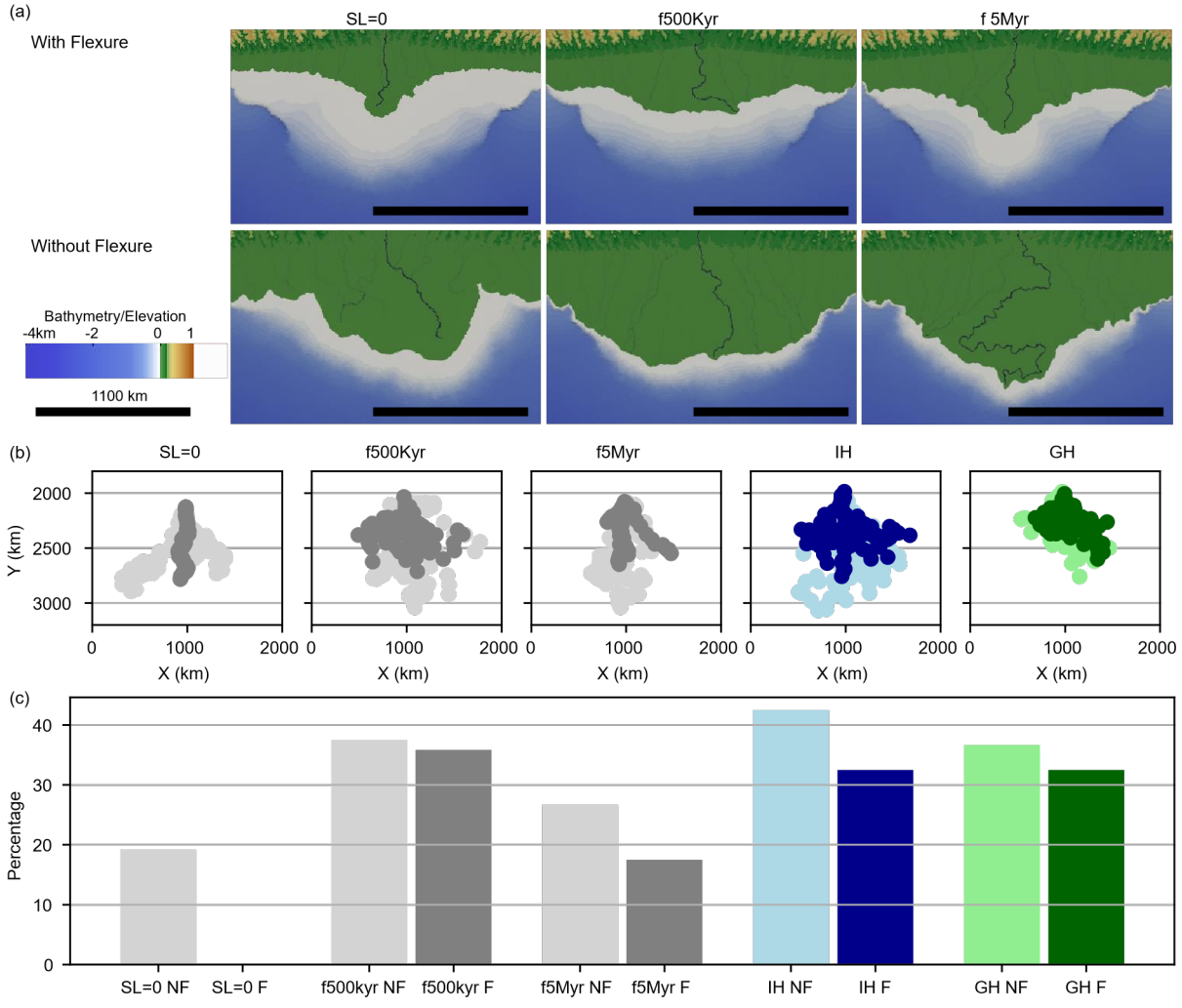

425

Figure 8. (a) Output of numerical simulations with imposed synthetic sea-level curves with different frequencies (f) showing elevation, bathymetry and discharge of the river mouth at 8 Myr. Note the difference in lateral extent, elevation due to flexural rebound, and river mouth morphology between the flexural (top) and non-flexural (bottom) cases. (b) Change of river mouth location though time for simulations where synthetic and empirical sea-level curves were imposed. Mean river mouth transit
430 **distances in the non-flexurally compensated simulations are shown in lighter shades, whereas the flexurally compensated cases are shown in darker shades. (c) Bar plot showing the frequency of the number of times where the de-trended river-mouth trajectory crosses an arbitrary point in the shelf an indicator of how often the river mouth is close to the shelf break. NF = non-flexural, F = flexural, IH = icehouse, and GH = greenhouse.**

https://doi.org/10.5194/egusphere-2023-53
Preprint. Discussion started: 3 March 2023

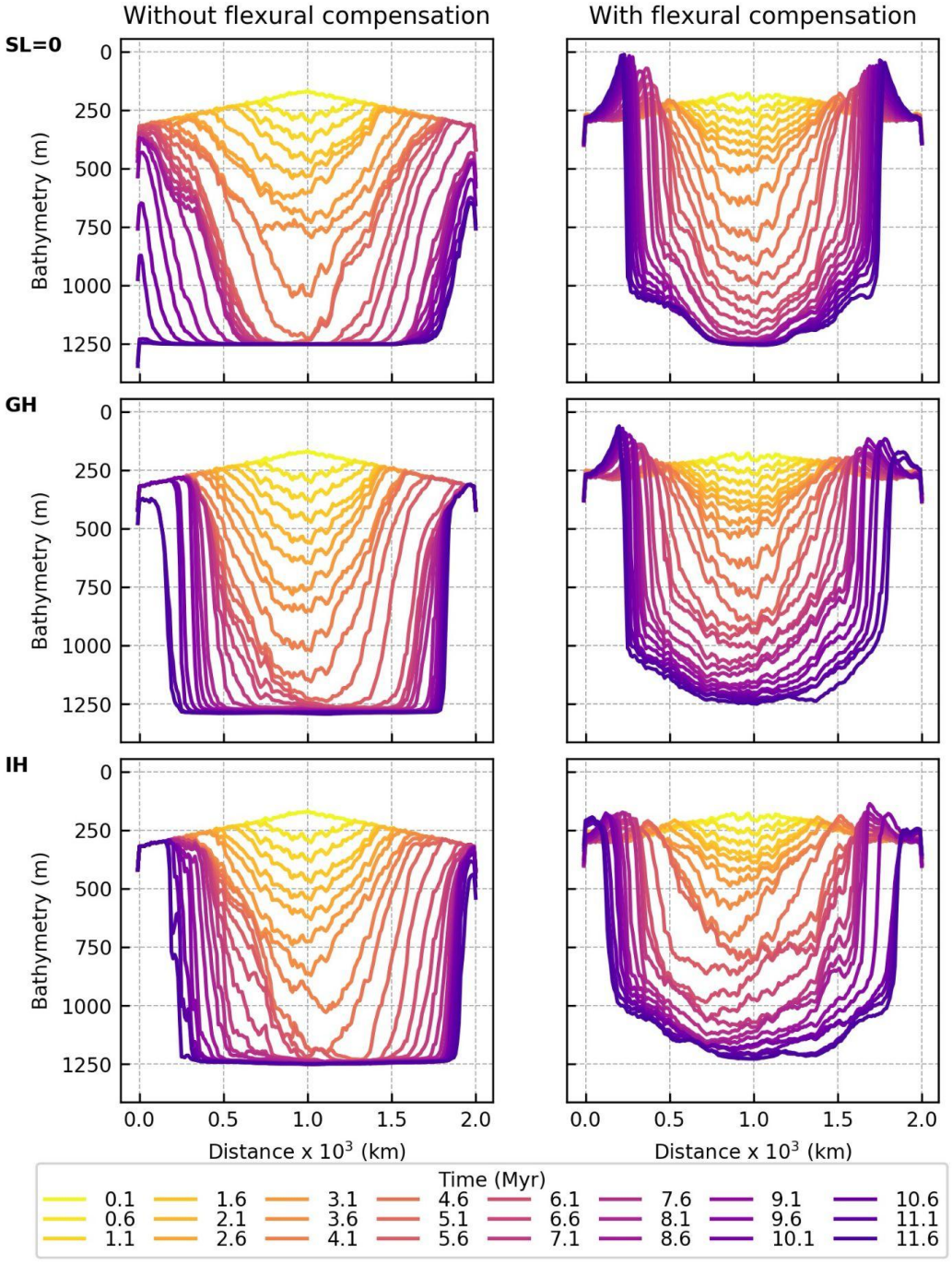

435 **Figure 9. Along strike cross-sections showing the comparison of the bathymetric evolution for simulations without (first column) and with (second column) flexural compensation for different sea-level scenarios. SL=0 constant sea-level, GH= greenhouse, IH= icehouse. The bulges on each of the sides of the deltaic depocenters are the result of the uplift generated by the flexural compensation while the curvature on the bottom of the depocenter is caused by the flexural deflection. Note how both the bulges and curvatures are absent in the simulations without flexural compensation.**

https://doi.org/10.5194/egusphere-2023-53
Preprint. Discussion started: 3 March 2023

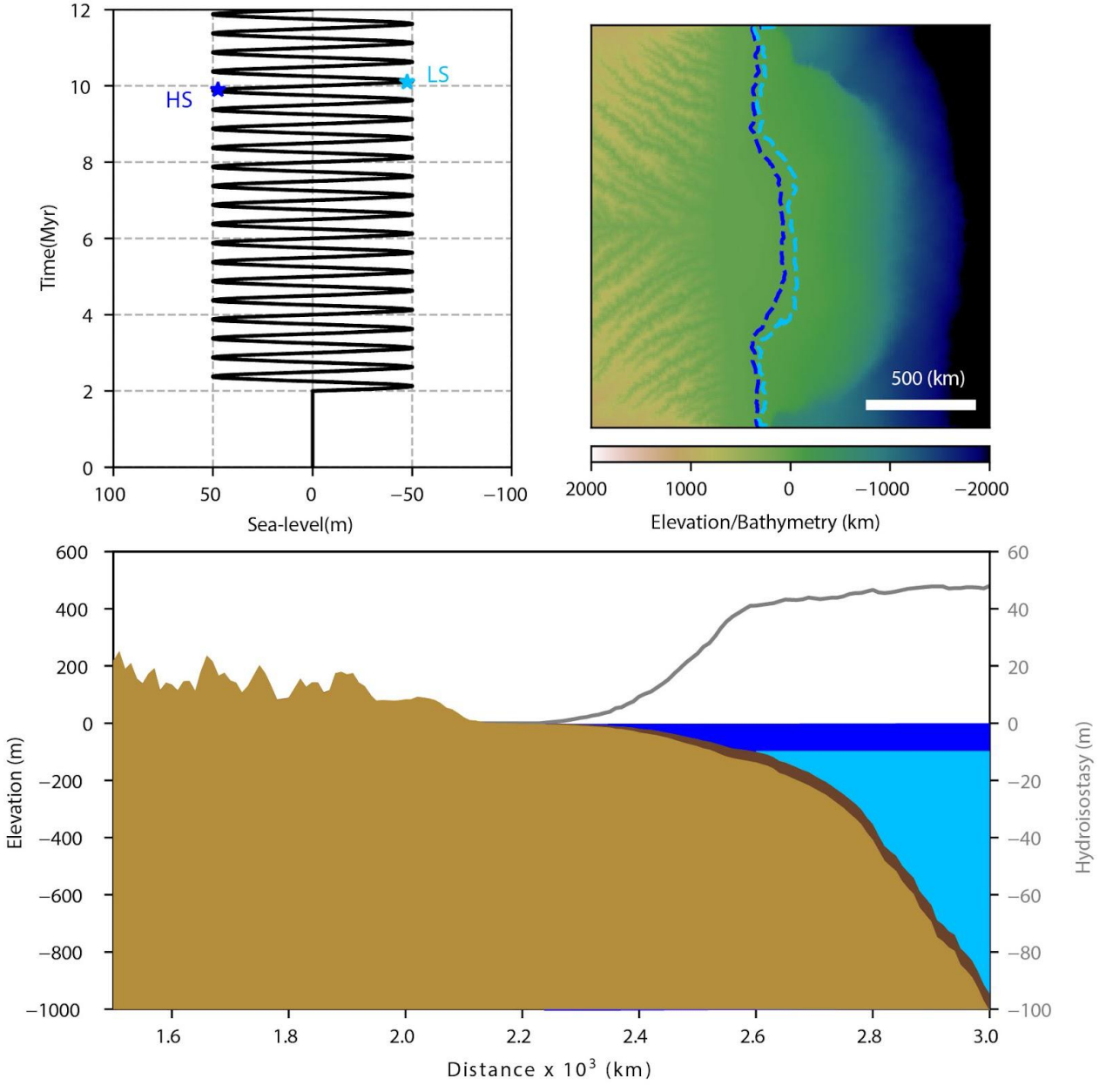

Figure 10. Model results showing the uplift generated by the hydro-isostatic adjustment associated with a sea-level fall of 100 m and exposure of the shelf. Left: Synthetic sea-level curve with an amplitude of 50 m and a frequency of 500 Kyr, the asterisks show the particular time step of the simulation where the results were extracted. HS = highstand (dark blue) LS = lowstand (light blue). Middle: output of numerical simulations showing elevation, bathymetry and shoreline position at HS (dark blue) and LS (light blue). Right: Longitudinal profile for HS (dark blue) and LS (light blue). Horizontal lines show the position of the sea-level. The vertical difference in bathymetry between the HS and LS can be explained by the uplift created by the hydro-isostasy (dashed gray line) related to the change in sea level between HS and LS. Model output elevation was adjusted to correspond to sea-level (or zero).

https://doi.org/10.5194/egusphere-2023-53
Preprint. Discussion started: 3 March 2023

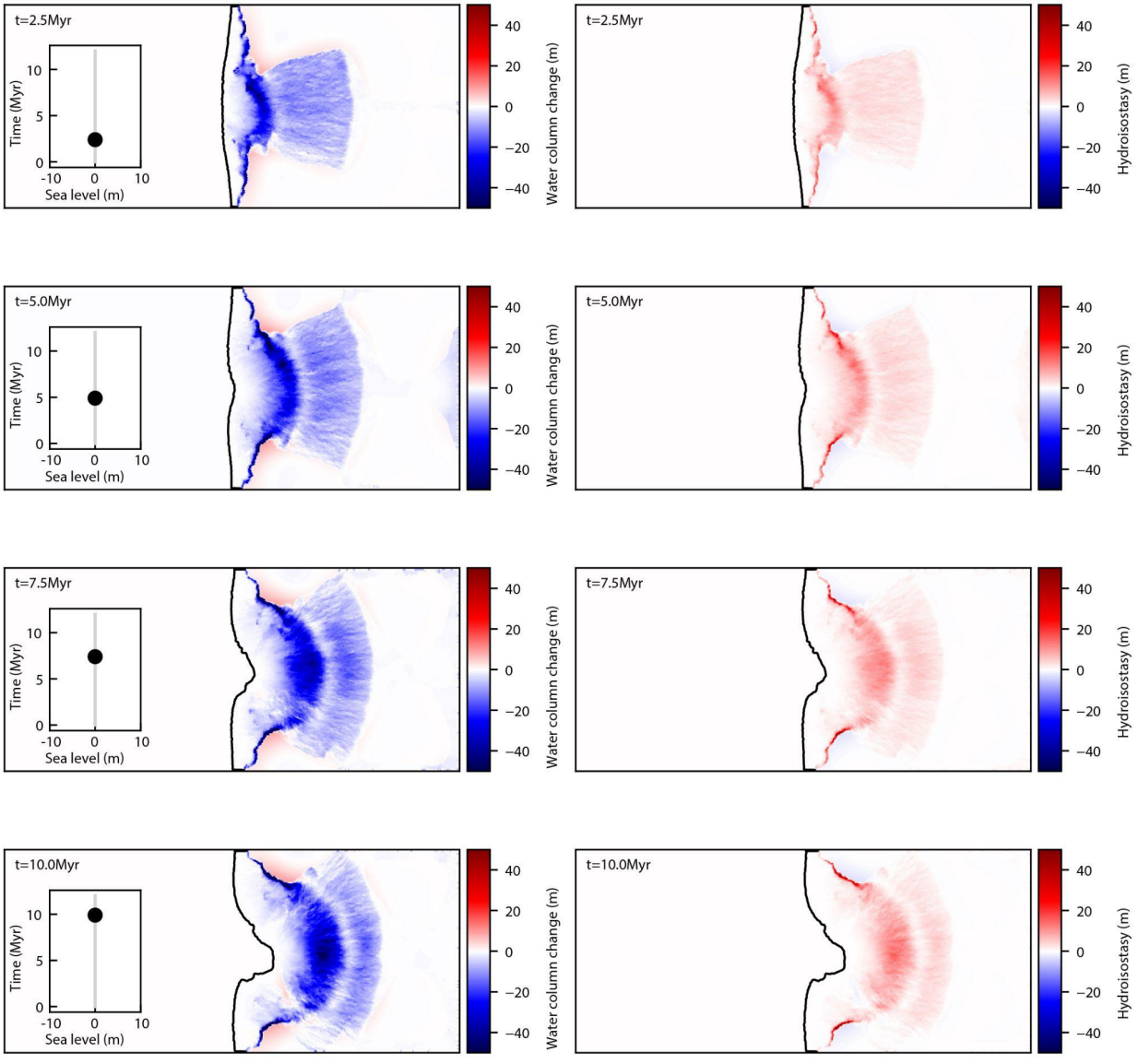

Figure 11. Map views showing the temporal evolution of the change in water column (left) and associated hydro-isostasy (right) in the numerical simulations with no sea-level change. Insets on the left panels show the imposed sea-level curve and the round symbol the point in time when the simulation output was taken. Because sea level is constant changes in relative sea level and hydro-isostasy are associated with the progradation of the sediment wedge which in turn causes variations in the gradient of the shelf edge' slope but not around the shoreline. Note how the hydro-isostasy is consistently positive through time.

https://doi.org/10.5194/egusphere-2023-53
Preprint. Discussion started: 3 March 2023

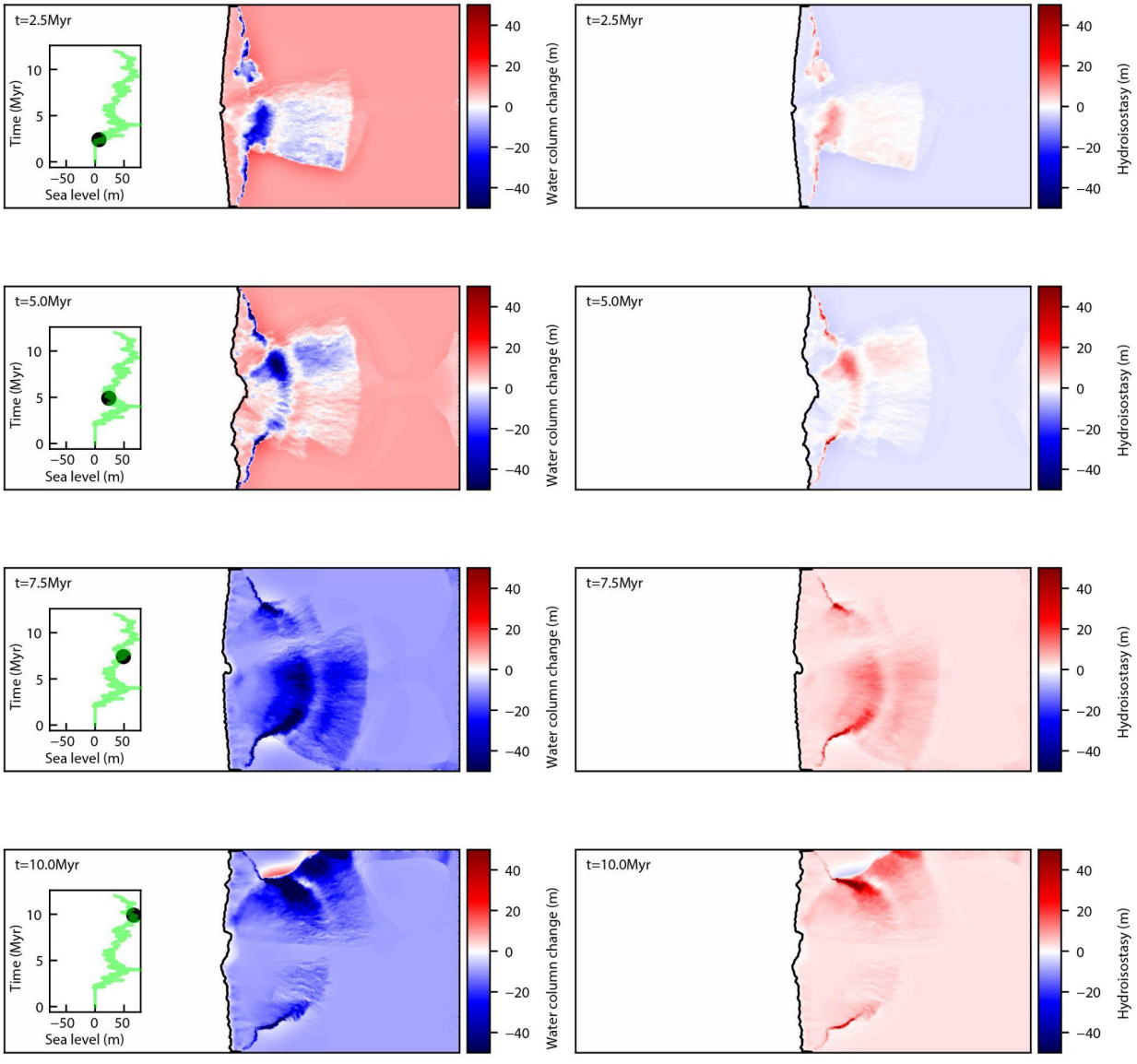

Figure 12. Map views showing the temporal evolution of the change in water column (left) and associated hydro-isostasy (right) in the numerical simulations with a green-house sea-level curve. Insets on the left panels show the imposed sea-level curve and the round symbol shows the point in time when the simulation output was taken. The spatial variation of the hydro-isostasy is a function of elevation changes as the sediment wedge progrades and fluctuations in sea level. Note the changes in the direction of hydro-isostasy through time, which contrasts with the results from the simulations with no sea-level change presented in the previous figure.

https://doi.org/10.5194/egusphere-2023-53
Preprint. Discussion started: 3 March 2023

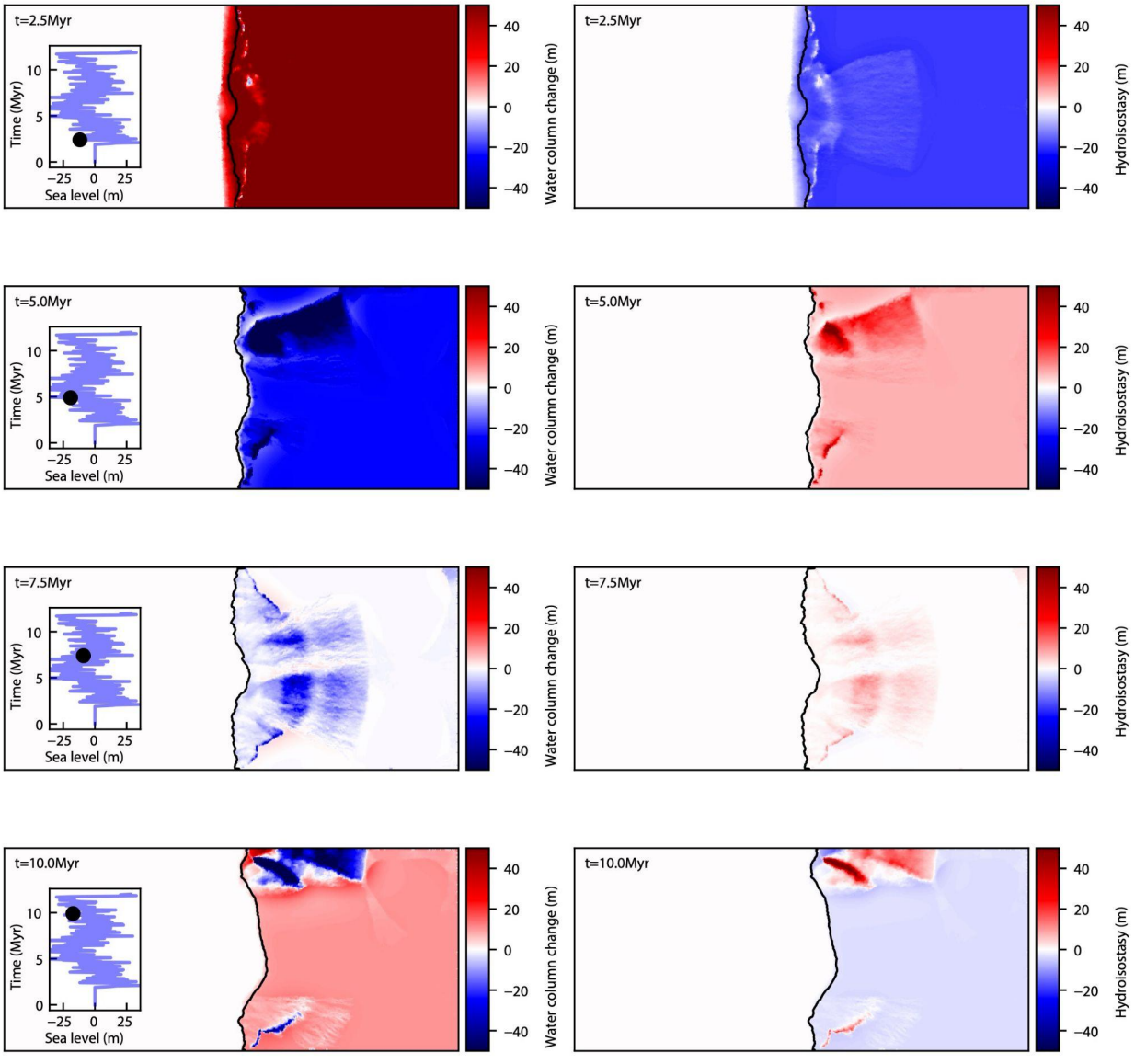

Figure 13. Map views showing the temporal evolution of the change in water column (left) and associated hydro-isostasy (right) in the numerical simulations with an ice-house sea level curve. Insets on the left panels show the imposed sea-level curve and the round symbol shows the point in time when the simulation output was taken. The spatial variation of the hydro-isostasy is a function of elevation changes as the sediment wedge progrades, the valley incision during sea-level fall and fluctuations in sea level. Changes in the direction of hydro-isostasy through time are more dramatic than on the numerical simulations with a green-house sea level curve.

https://doi.org/10.5194/egusphere-2023-53
Preprint. Discussion started: 3 March 2023

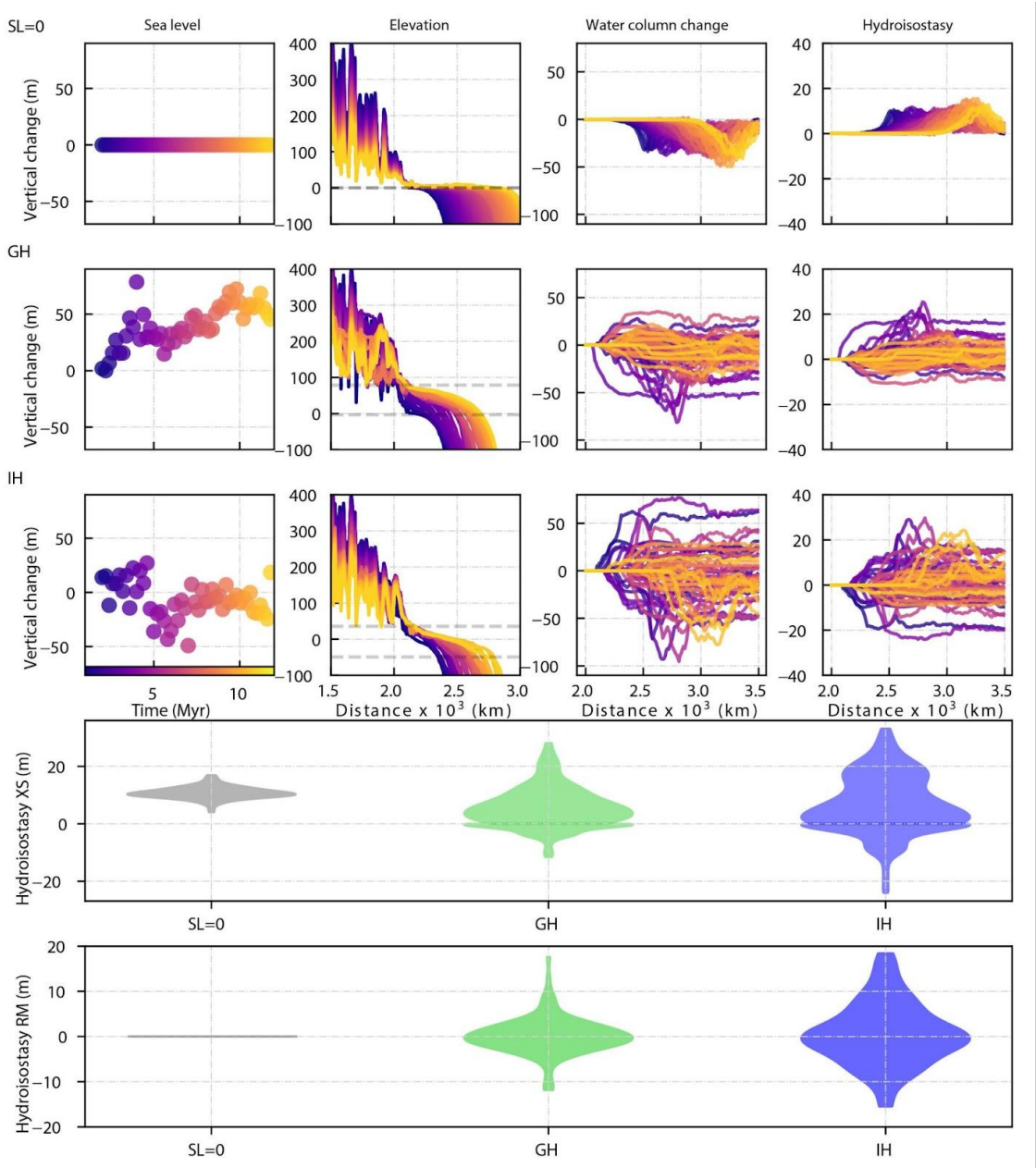

Figure 14. Temporal evolution of sea-level, elevation, water column change and hydro-isostasy along a down-dip section in the middle of the modeling domain for the simulations with different sea level scenarios: SL0=0 constant (first row), GH=greenhouse (second row), and IH=icehouse (third row). Changes in relative sea level and associated hydro-isostasy are related to the interplay between the progradation of the sediment wedge, flexural isostasy of the water and sediment load. The positive values in the hydro-isostasy fluctuate because of bathymetric changes caused by the progradation of the sediment wedge and flexural subsidence. show the minimum and maximum sea level for each of the scenarios. Violin plots (modified kernel density plots) show the range of hydro-isostasic adjustments for the three sea level scenarios along a cross-section (XS, fourth row) and at the river mouth (RM, bottom). Note how the largest range in the hydro-isostatic response occurs in the simulations where the ice-house sea level was imposed.

https://doi.org/10.5194/egusphere-2023-53
Preprint. Discussion started: 3 March 2023

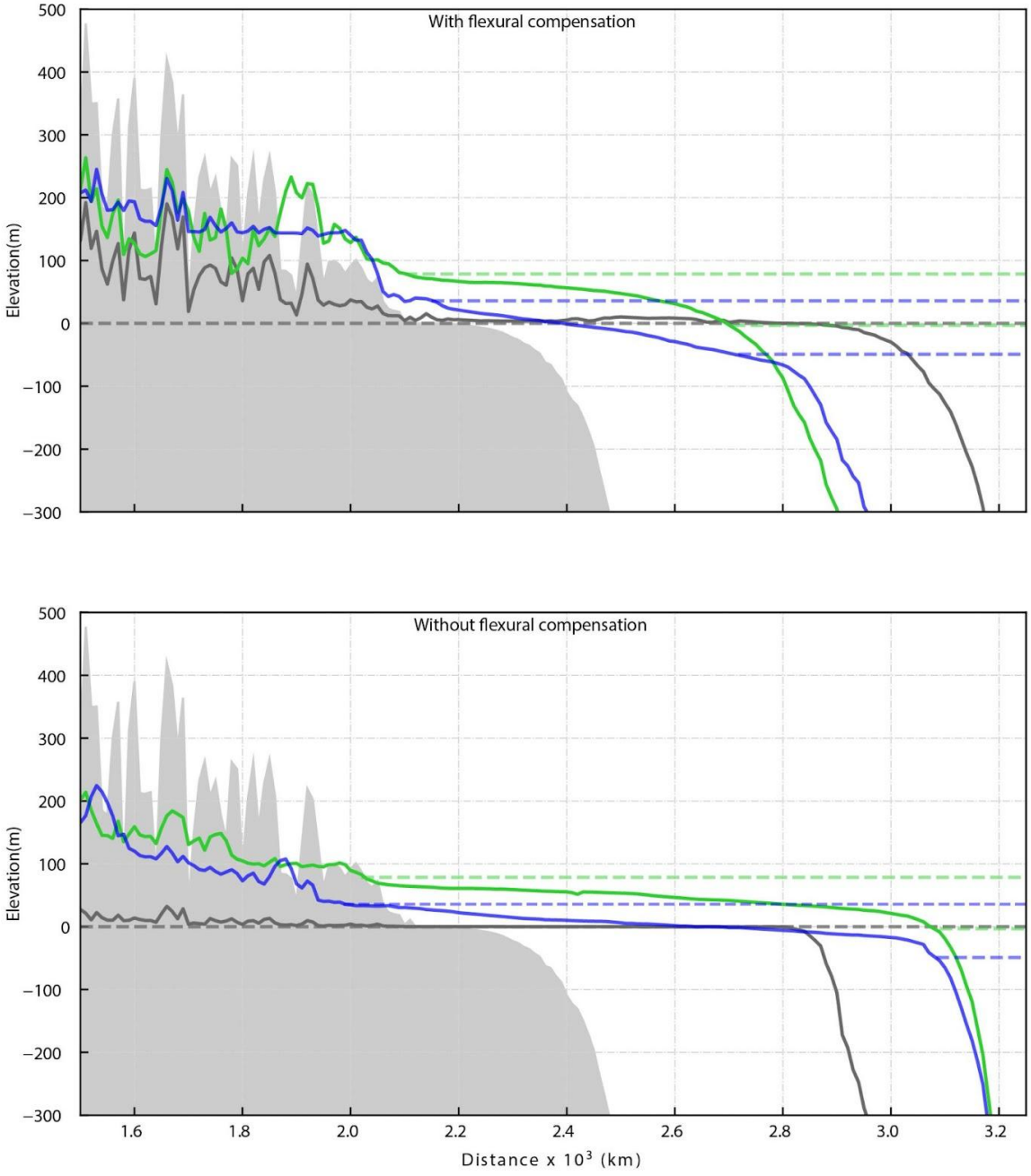

Figure 15. Comparison of the down-dip shelf slope profile for scenarios with no sea level change (dark grey) green house (green) and ice house (blue). Note how the shelf rollover depth adjusts to changes in sea-level amplitude and frequency. In the models without flexural compensation the final elevation of the coastal plain is the result of the initial topography, in that case only erosion and base-level changes control the vertical adjustments, as illustrated by the lack of relief in the case with no sea level change. Dashed lines show the minimum and maximum sea level for each of the scenarios.

https://doi.org/10.5194/egusphere-2023-53
Preprint. Discussion started: 3 March 2023

Table 1 Boundary conditions and input parameters used in the modeling simulations.

Simulation ID	Sea-level curve	Flexural Isostasy	Rain (myr-1)	Erodibility coefficient	Surface diffusion coefficient (m2/a)	Marine diffusion coefficient (m2/a)	River transported sediment diffusion coefficient in marine realm (m2/a)	Time step used to compute the isostatic flexure	Mantle density (km/m3)	Sediment density (km/m3)	Young's Modulus (Pa)	Grid resolution (m)
f500kry	Synthetic f=500 kyr, A=25 m	Te = 50 km	1	4.00E-07	3.00E-02	5.00E-02	2.00E+01	1.00E+05	3330	2170	1.00E+11	1.00E+04
f5Myr	Synthetic f=5 Myr A=25 m	Te = 50 km	1	4.00E-07	3.00E-02	5.00E-02	2.00E+01	1.00E+05	3330	2170	1.00E+11	1.00E+04
SL0	Constant	Te = 50 km	1	4.00E-07	3.00E-02	5.00E-02	2.00E+01	1.00E+05	3330	2170	1.00E+11	1.00E+04
f500kry NF	Synthetic f=500 kyr, A=25 m	-	1	4.00E-07	3.00E-02	5.00E-02	2.00E+01	1.00E+05	3330	2170	1.00E+11	1.00E+04
f5MyrNF	Synthetic f=5 Myr A=25 m	-	1	4.00E-07	3.00E-02	5.00E-02	2.00E+01	1.00E+05	3330	2170	1.00E+11	1.00E+04
SL0 NF	Constant	-	1	4.00E-07	3.00E-02	5.00E-02	2.00E+01	1.00E+05	3330	2170	1.00E+11	1.00E+04
IHF	33.9 Ma - 23.9 Ma, Miller et	Te = 50 km	1	4.00E-07	3.00E-02	5.00E-02	2.00E+01	1.00E+05	3330	2170	1.00E+11	1.00E+04

https://doi.org/10.5194/egusphere-2023-53
Preprint. Discussion started: 3 March 2023

	al., (2020)											
GHF	66.0 Ma - 56.0 Ma, Miller et al., (2020)	Te = 50 km	1	4.00E-07	3.00E-02	5.00E-02	2.00E+01	1.00E+05	3330	2170	1.00E+11	1.00E+04
IHNF	33.9 Ma- 23.9 Ma, Miller et al., (2020)	-	1	4.00E-07	3.00E-02	5.00E-02	2.00E+01	1.00E+05	3330	2170	1.00E+11	1.00E+04
GHNF	66.0 Ma - 56.0 Ma, Miller et al., (2020)	-	1	4.00E-07	3.00E-02	5.00E-02	2.00E+01	1.00E+05	3330	2170	1.00E+11	1.00E+04

495

https://doi.org/10.5194/egusphere-2023-53
Preprint. Discussion started: 3 March 2023

Table 2 Mean values for river mouth length and mean maximum accumulation values measured at each time step of the simulation. The statistics presented here are from 2Myr to 12Myr, which is when we imposed different sea-level fluctuations to simulations.

	Mean river mouth length (km) Non-Flexural simulations	Mean river mouth length (km) Flexural simulations	p-value	Mean maximum accumulation (m) Non-Flexural simulations	Mean maximum accumulation (m) Flexural simulations	p-value
SL=0	2538	2425	5.44E-05	961	1724	8.43E-09
f500Kyr A25m	2491	2340	3.64E-07	1188	1392	5.19E-02
f5Myr A25m	2523	2354	7.14E-07	1215	1702	2.22E-04
GH	2310	2250	2.00E-03	1067	1394	1.44E-03
IH	2561	2341	1.07E-11	1052	1415	4.16E-04

500

https://doi.org/10.5194/egusphere-2023-53
Preprint. Discussion started: 3 March 2023

Code availability

The model inputs and outputs as well the post-processing codes used in this study are available online at https://github.com/saraemp/egusphere-2023-53

Author contribution

SP Designed the simulations, carried them out and prepared the manuscript. MB contributed to the conceptual design of the simulations and the manuscript writing. TS significantly contributed to the performance of the simulations and code development. TS, RF, XD, BM and CM helped with the post-processing codes. All authors contributed to the revision and editing of the manuscript.